Ocean Dynamics (2011) 61:881–890
DOI 10.1007/s10236-011-0406-7

FESOM under coordinated ocean-ice reference experiment forcing

Dmitry Sidorenko · Qiang Wang · Sergey Danilov · Jens Schröter

Received: 14 December 2010 / Accepted: 9 March 2011 / Published online: 16 April 2011

Abstract Characteristics of the ocean state simulated with the Finite-Element Sea-Ice Ocean Model (FESOM) under the normalized year forcing of Coordinated Ocean-ice Reference Experiments (COREs; Griffies et al., Ocean Model 26:1–46, 2009) are compared with those of other models participating in COREs. In contrast to these models, FESOM is run on an unstructured mesh (with resolution varying between 20 and 150 km). It is shown that the ocean state simulated by FESOM is in most cases within the spread of other models, demonstrating that the unstructured mesh technology has reached the stage when it becomes a reliable tool for studying the large-scale ocean general circulation.

Keywords Finite elements · Sea-ice ocean model · COREs · Ocean general circulation

1 Introduction

The Coordinated Ocean-ice Reference Experiments (COREs) were conceived as a platform to study the behavior of a suite of global ocean-ice models under common forcing (Griffies et al. 2009). Their first phase (CORE I) dealt with the analysis of ocean state under a normalized year forcing repeated for 500 years (see Griffies et al. (2009) for detail). The knowledge of the spread in characteristics of simulated ocean circulation and understanding the factors behind it (both on model and forcing sides) is a premise for using the models in climate modeling.

The models participating in CORE I differ in their configurations and algorithms, e.g., resolution, vertical coordinates, and mixed layer parametrizations. The common forcing strategy accepted in CORE I does not imply that the models are driven with the same heat and fresh water fluxes. The fluxes are determined through bulk formulas and thus depend on the simulated ocean state. Besides, there is freedom in applying fresh water forcing. Two relaxation strategies with the piston velocity of 50 m/4 years and 50 m/300 days, respectively, were employed, augmented with the (optional) step of normalization (balancing the implied salinity or fresh water fluxes). Despite these obvious differences, every setup sought to reproduce a consistent, balanced ocean circulation.

Finite-Element Sea-Ice Ocean Model (FESOM) (Danilov et al. 2004; Wang et al. 2008; Timmermann et al. 2009) is a novel global ocean circulation model based on the finite-element approach and designed to work on unstructured meshes. Its main new feature lies in the ability to provide a regional focus in an otherwise global setup. Because of the unstructured mesh's functionality, its numerical core is distinct in many important ways from that of models formulated on regular meshes. In particular, the shape of stencils used to compute derivatives may vary from node to node, and viscosity and diffusivity coefficients are always scaled. A question arises as to what extent such a model can be used to simulate the large-scale ocean circulation on long-time scales.

Responsible Editor: Eric Deleersnijder

D. Sidorenko (✉) · Q. Wang · S. Danilov · J. Schröter
Alfred Wegener Institute for Polar and Marine Research, Bremerhaven, Germany
e-mail: Dmitry.Sidorenko@awi.de

In order to establish FESOM as a general-purpose ocean circulation model, the present study aims at understanding its long-term behavior under the climatological forcing of CORE I. In this sense, we follow the proposal of Griffies et al. (2009) to use COREs as "a common reference point for research groups developing and analyzing global ocean-ice models." To be close to other models in terms of resolution, we use a mesh with only mild refinement in the equatorial belt and in the vicinity of coastlines. We demonstrate that despite the uncommon technology, FESOM simulates an ocean state that is generally within the spread demonstrated by other CORE I participants.

The motivation for the diagnostics selected in COREs and relevant critical issues are discussed in Griffies et al. (2009) and will not be repeated here. We start from a brief description of the FESOM setup used here. It will be followed by the intercomparison and conclusions.

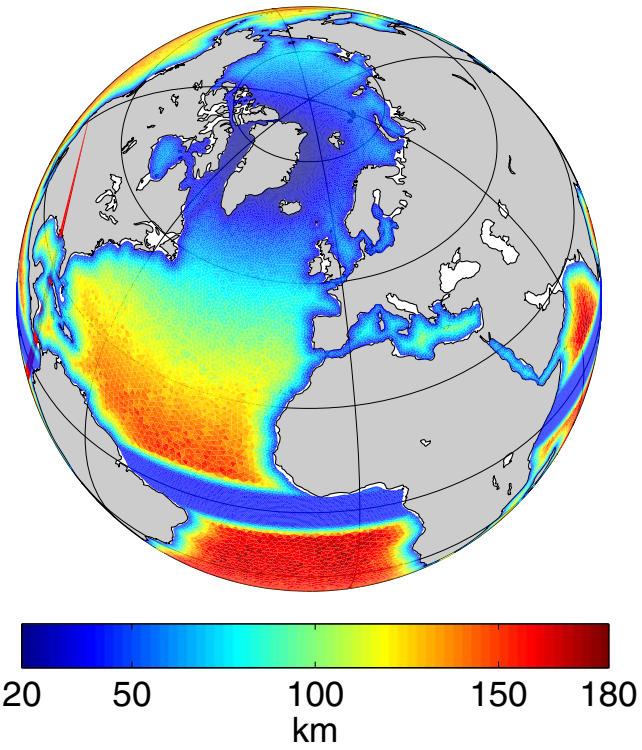

Fig. 1 Mesh resolution over the model Atlantic sector. It is about 150 km in the interior, 40 km in the equatorial belt, and about 20 km along the coastlines and in the vicinity of Greenland

2 FESOM setup

Certain aspects of FESOM design are still subject to change, but they do not depart significantly from the numerical core described by Wang et al. (2008). The setup used here employs z-coordinates, triangular unstructured surface mesh, and tetrahedral volume elements. In this latter respect, it deviates from the description in Wang et al. (2008) which assumes prismatic elements. The mesh nodes are vertically aligned, as in structured-mesh models, to avoid difficulties in resolving the hydrostatic balance. The tetrahedral elements are obtained through splitting the triangular prisms defined by the surface mesh and level surfaces. Although the number of tetrahedral elements is approximately three times larger than that of prismatic elements, they admit a linear representation of the model fields for any generalized level surfaces. This has some advantages for programming and does not affect the computational efficiency (in some situations, it can also lead to disadvantages, mostly linked to anisotropy of stencils in the vertical direction; the relevant details will be discussed elsewhere). The (finite-element) sea-ice component of FESOM is briefly sketched in Timmermann et al. (2009). It employs the surface mesh of the ocean component.

The model is configured on a longitude–latitude mesh rotated so that poles are in Greenland and in the Antarctic continent and uses variable resolution from about 150 km in the open ocean to 20 km along coastlines and, because of convergence of meridians, in some vicinity of Greenland (see Fig. 1). The latter contributes to an improved representation of the Denmark Strait. Additionally, the mesh is refined in the equatorial belt to about 40 km. There are 39 vertical levels. The presence of relatively small elements imposes limitations on the time step which is 45 min. The horizontal Laplacian viscosity and isopycnal diffusivity are parameterized as ΔV where $V = 0.06$ and $0.006\ \mathrm{ms}^{-1}$, respectively, and Δ is the square root of element surface area. The Redi (1982, Redi) diffusion and the Gent and McWilliams (1990, GM) parametrization are applied with the critical neutral slope of 0.004. The GM parametrization is implemented following Griffies (1998). The skew diffusivity is the same as the Redi one.

Originally, the isopycnal slope was calculated on tetrahedral elements of model domain discretization, which is consistent with the way how temperature and salinity gradients are estimated. Unexpectedly, the bottom cell of meridional overturning circulation was found to be too strong in that case (see Timmermann et al. (2009) for an example), which possibly has links to non-uniformity of computational stencils of tetrahedral discretization. In this work, the isopycnal slope is computed on parent triangular prisms that the mesh is composed of before splitting into tetrahedral elements.

In this case, the strength of the bottom cell is comparable to that of most models analyzed in Griffies et al. (2009).

Vertical mixing is provided by the Pacanowski and Philander (1981) scheme with the background vertical diffusion of 2×10^{-3} m^2 s^{-1} for momentum and 10^{-5} m^2 s^{-1} for the potential temperature and salt, and maximum value limited to 0.01 m^2 s^{-1}. The additional mixing scheme by Timmermann et al. (2002) is introduced (the diffusivity of 0.01 m^2 s^{-1} is applied over a depth defined by the Monin–Obukhov length) in order to avoid unrealistically shallow mixed layers in summer. The forcing implementation follows that of Griffies et al. (2009). It includes turbulent fluxes for heat (sensible and latent), water (evaporation), and momentum (wind stress), radiative heat fluxes (shortwave and longwave) and water fluxes such as precipitation, river runoff, and sea-ice formation/melt.

FESOM can be run with a full nonlinear free surface. However, in contrast to finite-difference and finite volume models, updating the upper layer thickness implies updating mass matrices, the elevation stiffness matrix and the arrays of derivatives, which creates additional computational burden. If semi-implicit time stepping is used then, as a rule, the preconditioning must be performed every time step for the updated matrices, which takes time. The upper bound of the associated overhead can easily surpass a twofold level. In the current setup, however, the cost of switching on the nonlinear free surface option does not exceed 10% of the total cost. Hence, to warrant efficiency, the simulations were performed with a linear free surface and, consequently, with implied salinity forcing. The piston velocity in the haline surface forcing was selected as 80 m/4 years, which is only slightly higher than the weak forcing of COREs, and normalization of virtual salinity flux was performed after each complete year.

We note that the finite-element placement of variables in FESOM is equivalent to A-grid in all directions. This implies that the surface temperature, salinity, and velocity are taken at the surface and not at the mid-depth of the first cell. This can introduce some bias with respect to traditional practices.

3 Comparison results

3.1 Temperature and salinity

The diagnostics performed in this and subsequent sections follow the analysis of Griffies et al. (2009). We begin with the behavior of globally averaged temperature and salinity shown by blue (temperature) and green (salinity) curves in Fig. 2a as functions of time. It has to be compared with Figs. 3 and 4 of Griffies et al. (2009). Note that evolution of these quantities is entirely due to the lack of balance in ocean surface fluxes. Nevertheless, it is expected that the equilibrium will be reached after some (long) adjustment phase. This is indeed the case for most models of CORE I (except for KNMI-MICOM and GFDL-HIM). In the FESOM case, the mean global temperature does not reach the equilibrium state after 500 years exhibiting an almost constant trend of slightly more than −0.01°C per 100 years over the last 200 years of the integration time. FESOM however completes the 500-year simulation with the mean temperature of 3.76°C which is in between the mean temperature spread of other models.

In contrast, salinity exhibits a linear trend of about −0.006 psu per 100 years over the whole period of integration. This trend is lower than that of KNMI-MICOM and GFDL-HIM (about −0.03 psu per 100 years) but differs from other z-coordinate simulations. Kiel-ORCA shows a positive linear increase in salinity slightly less than 0.004 psu per 100 years while other models demonstrate almost zero trend. The trend in FESOM is presumably linked to weak relaxation of model salinity to climatological values and flux normalization on rather long (annual) time scale. The salinity at the end of integration is 34.685 psu, close to the lower limit of other model solutions, and lower than the value (34.72 psu) of models with nearly no trend.

A deeper insight into the temperature and salinity evolution can be derived from the horizontally averaged fields. Figure 2c, d shows the horizontally averaged fields as functions of depth and time for temperature and salinity, respectively. The initial profile has been subtracted from the time series to visualize the variability. Similarly to other models, the main adjustment of temperature occurs within the first 200 years in the thermocline. The upper ocean becomes warmer while the deeper ocean remains almost intact. FESOM variability resembles that of the FSU-HYCOM simulation most closely. The negative salinity change is localized within the upper thermocline, but with time a small anomaly penetrates also into the deep ocean.

Deviations of model sea surface temperature (SST) and salinity (SSS) from climatology of Conkright et al. (2002) are shown in Fig. 3b, d, respectively. The model output has been averaged over the last 10 years of the simulation. The SST pattern shows a systematic warming over the large part of the ocean, with localized regions of cooling mostly confined to the Labrador

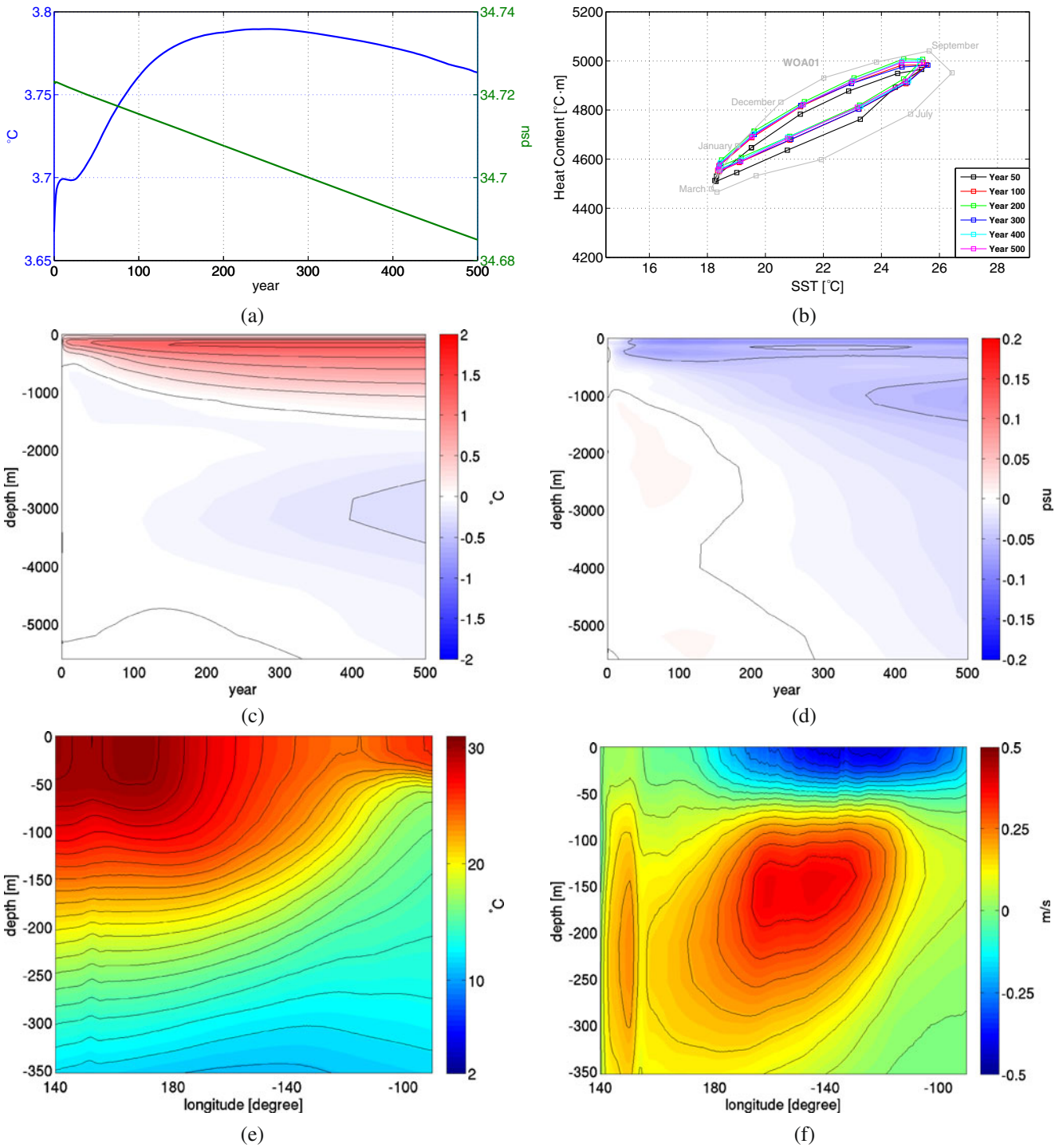

Fig. 2 **a** Time series of the globally averaged temperature (*blue curve*) and salinity (*green curve*). **b** Annual loop of heat content storage in the upper 250 m plotted against the surface temperature at (48° W and 35° N). Loops are shown for the year 50 and every 100 years. *Gray curve* corresponds to Conkright et al. (2002) climatology. **c**, **d** Time series of the zonally averaged temperature and salinity profiles, respectively. **e**, **f** Mean temperature and zonal velocity, respectively, for the last 10 years along the equatorial section in Pacific

and Nordic seas. As in many models of similar and even finer resolution (see e.g., Willebrand et al. 2001), the circulation simulated by FESOM shows the Gulf Stream displaced towards the western coast from its true position. This displacement leads to a shift in front position and is seen as a dipole of cold and warm

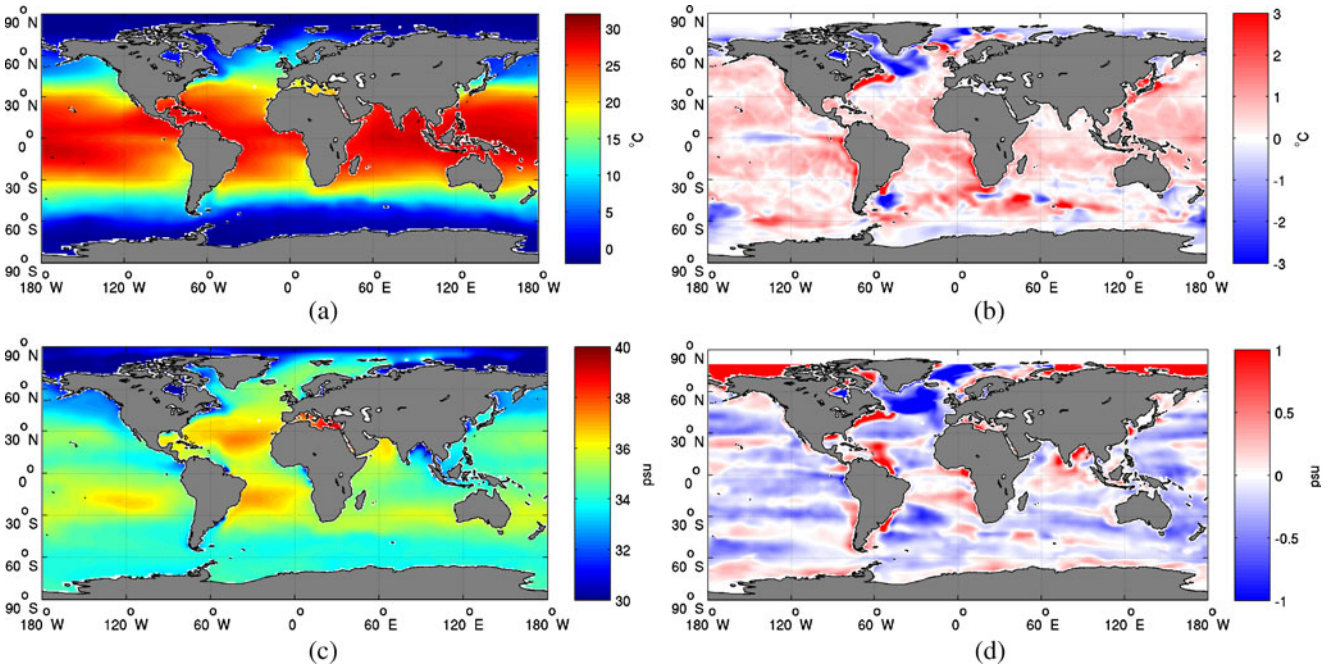

Fig. 3 **a**, **b** Annual mean SST from Conkright et al. (2002) climatology and the difference between the model (average over the last 10 years) and climatology, respectively. **c**, **d** The same as in the *upper panel* but for salinity

anomaly. This artifact is present in all models participating in COREs (see Figs. 7 and 8 of Griffies et al. 2009).

FESOM does not show a pronounced pattern of cooling in the central equatorial Pacific seen in other COREs simulations. The negative temperature anomaly over the upper North Atlantic is a feature which FESOM shares with all COREs models. The SST drift in FESOM is similar to that in MPI. SSS shows freshening over a considerable part of the global ocean. Notably, there is a rather strong freshening within the North Atlantic subpolar gyre, which probably has projection on a relatively thin mixed layer depth there and somewhat weak meridional overturning cell, as discussed further. Salinity increase is observed directly towards the Bering Strait, in the equatorial Atlantic and over a few other locations.

The following diagnostics in the COREs deals with the annual cycle at the Ocean Weather Ship Echo in the subtropical Atlantic at (48° W, 35° N). The annual cycle of heat content (computed as vertically integrated temperature) over the upper 250 m and SST at that location is compared with that computed from climatology of Conkright et al. (2002) (the monthly mean values are used). The hysteresis loops are presented in Fig. 2b which should be compared with Fig. 9 of Griffies et al. (2009). The cycle of heat storage and SST reaches an equilibrium relatively fast, already after 100 years of integration. The area and the position of the loop compares well to that of COREs. Despite relatively weak salinity restoring the position of the loop is within that from Conkright et al. (2002). This is a somewhat surprising result given the small piston velocity as MPI demonstrates a significant drift of this loop towards the lower heat content by reducing the piston velocity from 50 m/300 days to 50 m/4 years.

The thermal structure and upwelling in the tropical Pacific are important features contributing to model's ability to truly reproduce ENSO events in climate simulations. The section through the equatorial upper ocean in Fig. 2e shows mean temperature over the last 10 years of simulations. The core of the warm water is located in the upper layers at the western part of the domain and is above 30°C, in some contrast to other models (see Figs. 13 and 14 of Griffies et al. 2009), where it remains somewhat cooler. The coldest temperature at 350 m depth is above 10°C. In general, the pattern and the temperature range agree well with other findings (see e.g., Johnson et al. 2002) and the results in Griffies et al. (2009). The temperature pattern in FESOM is close to those from MPI, GFDL-MOM, GFDL-HIM, NCAR-POP and Kiel-ORCA models.

The corresponding zonal velocity in the same section is presented in Fig. 2f. FESOM shows the undercurrent with a maximum of about 0.4 m/s. This agrees with

the results of MPI model and FSU HYCOM, but is less than the observed values and also almost twice less than in other simulations. Low zonal velocities in MPI have been attributed to a lack of meridional resolution (about 1.7 degrees) in the tropical Pacific. Although the resolution in FESOM is roughly 0.5° within 5° equatorial belt (gradually decreasing to about 1.5 outside it), this alone is seemingly insufficient to improve the representation of dynamics.

The shape of the main core is also different from the other runs and is less inclined towards the upper ocean in the western part of the section. FESOM simulates a strong westward upper flow of 0.5 m/s. This flow is present in all other simulations and is commonly stronger than implied by observations. According to Griffies et al. (2009) this artifact in the zonal current pattern might be linked to the deficiency in the wind data.

One more diagnostic involves the analysis of zonally averaged maps of potential temperature and salinity. The differences between the mean model state over the last 10 years of simulation and climatology are shown in Fig. 4b, d for temperature and salinity, respectively (to be compared with Figs. 16 and 17 of Griffies et al. 2009). Similar to the most of COREs models FESOM shows systematic warming of the upper waters (above 1,000 m depth). Three main cores of warm anomalies are visible, with their centers at 40° S, the equator and 40° N. Similar pattern is simulated by the MPI model. The pattern of warming correlates with that of decreased salinity in many places. The northern part of the map shows the zonal cooling and freshening of

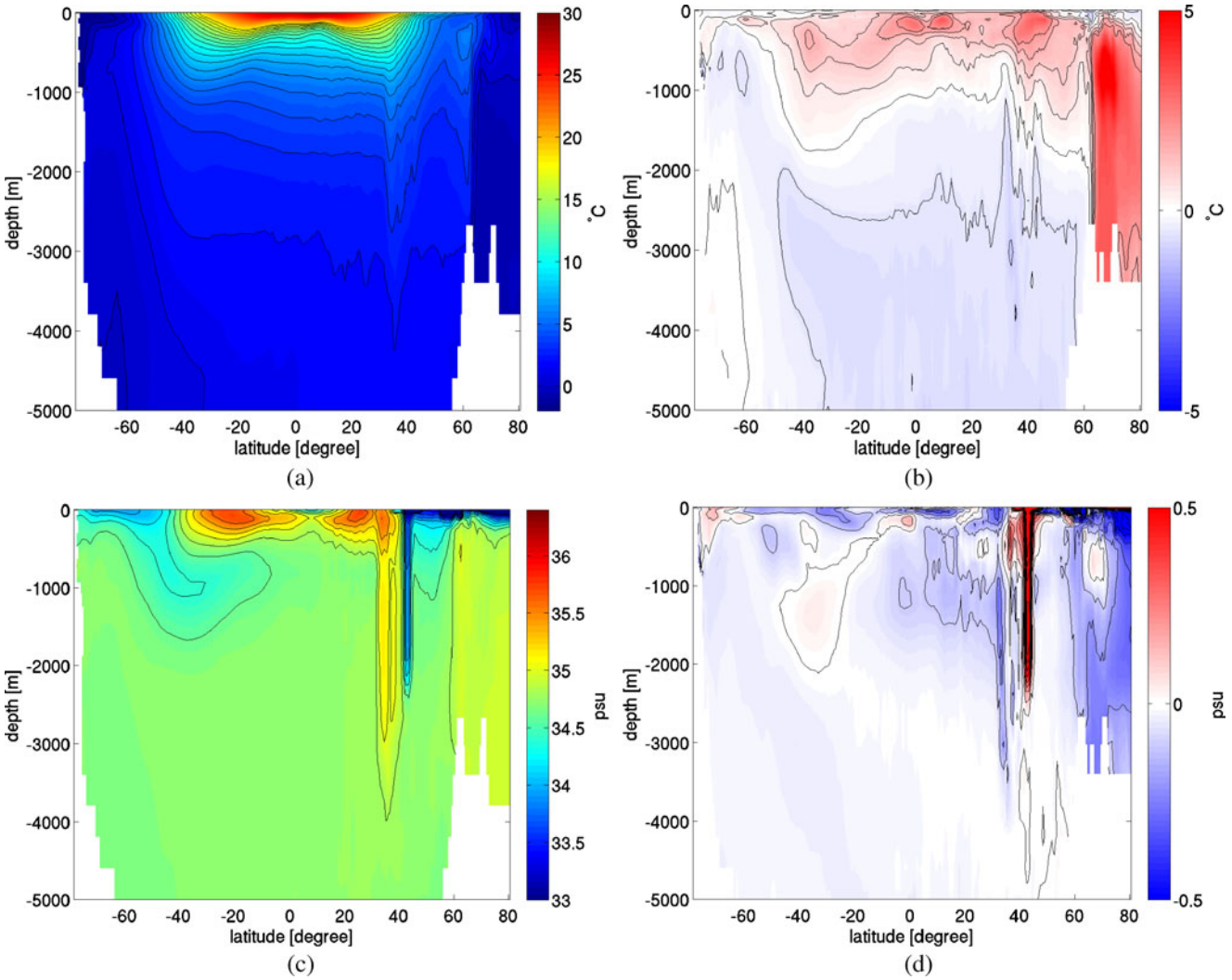

Fig. 4 **a**, **b** Zonally averaged annual mean temperature from Conkright et al. (2002) and the difference between the model (time mean for the last 10 years of the experiment) and the climatology, respectively. **c**, **d** Same as in the *upper panel* but for salinity

about 4°C and 0.5 psu, respectively. The same anomaly is exhibited by other models and is most pronounced in the MPI simulation. Similar to MPI, FESOM run shows the cooling trend in the deep ocean.

3.2 Ice

Reliable simulation of ice in polar regions is one of challenging tasks in climate modeling. Ice formation and melting strongly influence the ocean dynamics both locally in polar regions and, through the contribution of high-latitude processes in deep water production, in the world ocean. Figure 5 (to be compared with Fig. 10 of Griffies et al. 2009) presents the ice concentration integrated over the southern (green curve) and northern (blue curve) hemispheres as functions of time. Annually averaged values are shown. The northern ice area reaches the equilibrium already after 50 years and is about 9.8×10^{12} m^2. This is within the range reported by other CORE participants. KNMI-MICOM shows the ice coverage of 5×10^{12} m^2 and sets the lower boundary of the spread. MPI sets the upper boundary providing the ice area of 12×10^{12} m^2.

In the southern hemisphere, FESOM shows a multidecadal oscillations in ice coverage with a small positive trend within the last 200 years. FESOM ends up the simulation with an ice area of slightly less than 8.5×10^{12} m^2. The lower boundary in the southern ice coverage is once again defined by KNMI-MICOM and is about 5×10^{12} m^2. The upper boundary is 12×10^{12} m^2 as simulated by MPI and NCAR-POP models.

The sea-ice extents, defined by the areas of ice with concentrations at least 20% are 12×10^{12} m^2 for the northern and 15×10^{12} m^2 for the southern hemispheres, respectively. The northern extent compares perfectly with observations of about 12×10^{12} m^2 (see e.g., Cavalieri et al. 2003). The southern ice extent is larger than the observation by about 3×10^{12} m^2.

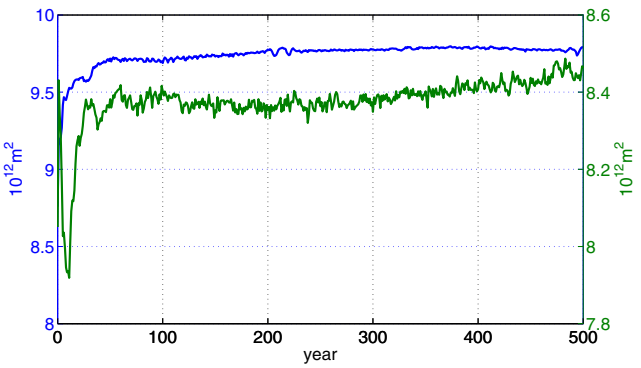

Fig. 5 Integrated sea-ice concentration over the Southern *green curve* and the Northern *blue curve* hemispheres as functions of time

The maps of ice concentration are shown in Fig. 6a, b for Northern and Southern hemispheres, respectively. They have to be compared with Figs. 11 and 12 of Griffies et al. (2009). The northern ice extends to above 60° N in March and retreats to slightly less than 70° N in September. Both northern patterns compare well to other participating models. The same is true for the southern patterns. However, the ice concentration in March is relatively low with noticeable ice presence only over the Weddell and Ross seas; in September it extends to 60° S over the Atlantic sector.

3.3 Poleward heat transport

The average of the model velocities over a sufficiently large time leads to the flow with zero transport divergence. This in turn implies that the oceanic heat transport across the specific latitude y equals to the integrated surface flux Q south of this latitude:

$$\rho_0 C_p \int \int_{-H}^{\eta} (vT)\mathrm{d}z\mathrm{d}x = \int_{y_s}^{y} \int Q\mathrm{d}x\mathrm{d}y, \qquad (1)$$

where ρ_0 is the reference density, C_p the specific heat, η the surface elevation, v the meridional velocity, T the temperature, y_s the southern boundary of the model domain, and x the longitude.

In the model run, the flux Q applied at the surface depends on the model state itself, forming a "feedback" between the ocean and prescribed atmosphere. Besides being of importance to climate studies it serves as a good benchmark for the model validation. We follow Griffies et al. (2009) and derive the heat transport from the LHS of Eq. 1 for the model fields averaged over years 491 to 500. The result is shown in Fig. 7. The poleward heat transport in the Northern Hemisphere slightly exceeds 1.5 PW at maximum. It reaches a smaller amplitude in the Southern Hemisphere. This agrees with the COREs and estimates of Trenberth and Caron (2001). Similar to other COREs simulations FESOM shows a deeper minimum than Large and Yeager (2004) (it is about −0.5 PW in their case). The zero line is crossed at equator and the maximum (minimum) are found between 10°–20° N (10°–20° S).

3.4 MOC/ACC transports

Transports, in particular the meridional overturning circulation (MOC), are frequently used to judge the model performance. They are part of COREs diagnostics too. The global MOC streamfunction of FESOM, averaged over last ten years of simulations, is shown in

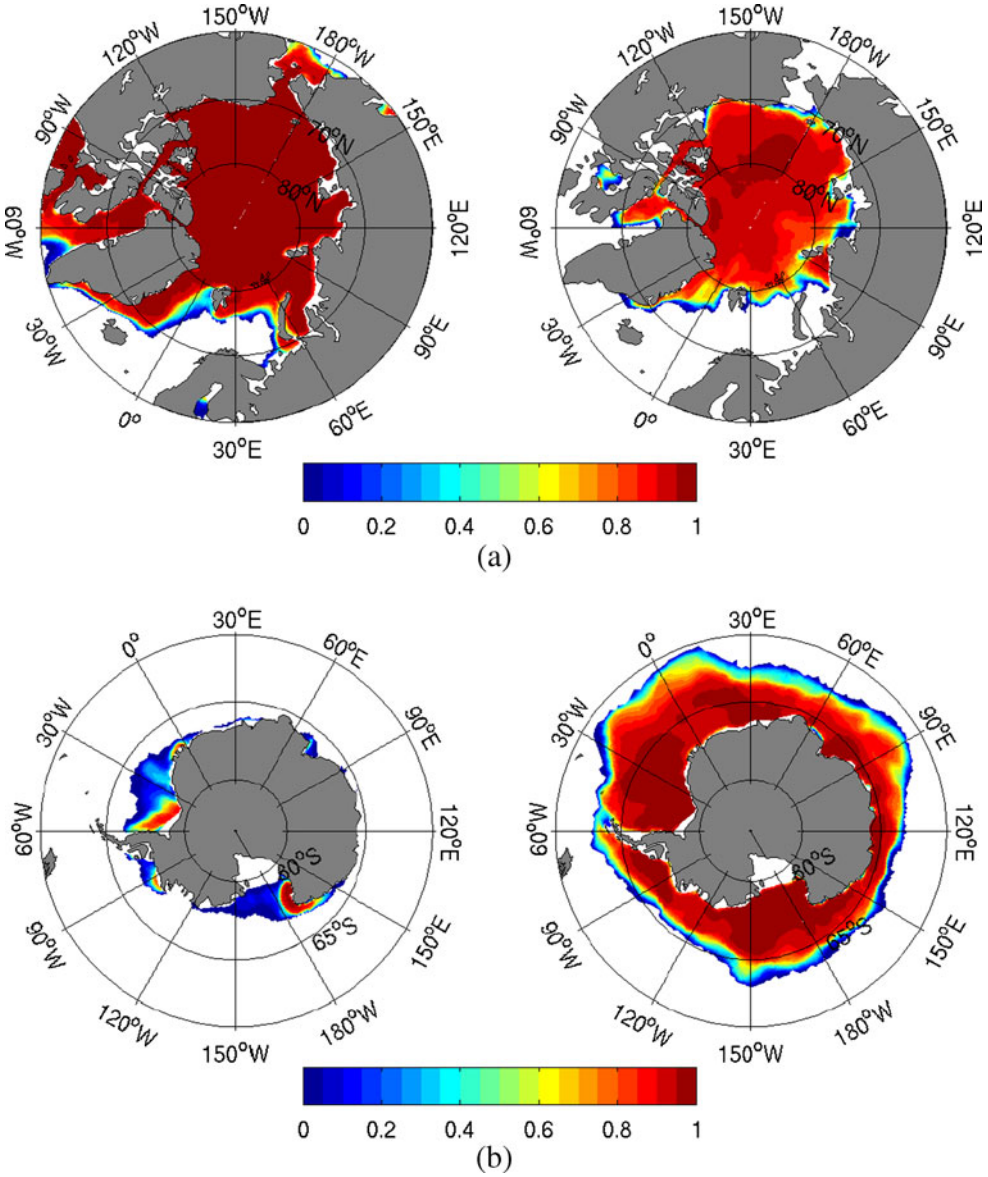

Fig. 6 **a**, **b** Mean sea-ice concentration for the last 10 years of the experiment in March (*left*) and September (*right*) in the Northern and Southern hemispheres, respectively

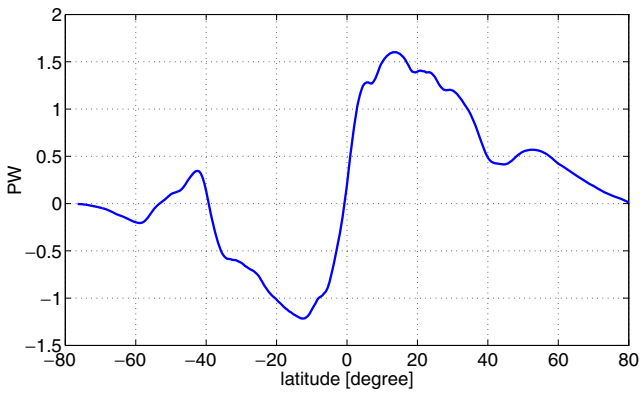

Fig. 7 Mean poleward heat transport for the last 10 years of integration

Fig. 8a. It has to be compared with Fig. 24 of Griffies et al. (2009). The middepth cell is of about 12 Sv in the North Atlantic sector. It underestimates the value reconstructed from observational data in the North Atlantic at 26.5° N (see e.g., Cunningham et al. 2007) by about 6 Sv, but still matches the results of other models, comparing to the MPI model most closely. Time series of its maximum value (reached at approximately 45° N) together with the volume transport across Drake Passage are given in Fig. 8b (to be compared with Fig. 18 of Griffies et al. (2009)). The MOC shows a continuous basinwide middepth cell with the northern maximum of about 11 Sv at 45° N. Although this value agrees with those from COREs models it is on the lower bound of their spread. This can be linked to the weak haline relaxation used in the FESOM run (80 m/4 years), as

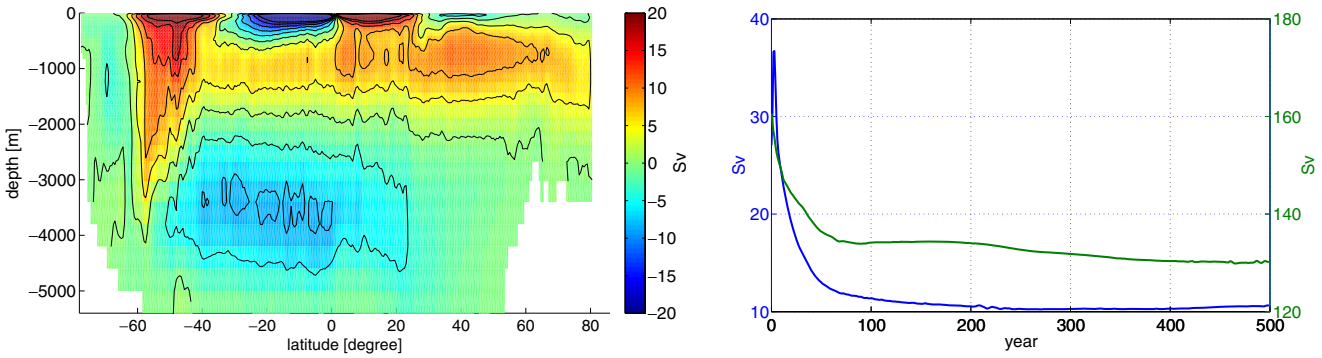

Fig. 8 **a** MOC streamfunction, mean over last 10 years model run. **b** Maximum of MOC at 45° N (*blue curve*) and Drake Passage transport (*green curve*) as functions of time

suggested by the sensitivity of MOC to the strength of salinity restoring reported for MPI and GFDL-MOM in Griffies et al. (2009). Another reason can be associated with reduced convective activity within the North Atlantic subpolar gyre which we observe in FESOM output. The bottom circulation cell is slightly less than 10 Sv, which agrees perfectly with the spread. Overall MOC produced by FESOM is similar to those of MPI, NCAR-POP and GFDL-MOM. The time series of the MOC maximum at 45° N in Fig. 8b (blue curve) shows that the meridional circulation reaches its equilibrium after about 100 years of integration.

The green curve in Fig. 8b plots the transport through the Drake Passage. It reaches an equilibrium of about 130 Sv at approximately the same time scale and compares well with real world observations of 130 ± 13 Sv (see e.g., Whitworth et al. 1982; Whitworth 1983; Whitworth and Peterson 1985) defining the median of the COREs spread.

3.5 Mixed layer depth

The last diagnostic of our analysis is the mixed layer depth (MLD) shown in Fig. 9 (cf Fig. 15 of Griffies et al. 2009). It is computed as the maximum monthly averaged MLD over the last ten years of simulation. Similarly to the MLD patterns of other participating models, it reveals a deep winter mixed layer over the Nordic seas. However, the MLD of FESOM is relatively thin over most of subpolar gyre, in some contrast to other models. The deep convection in the Labrador Sea is nearly absent. The model MLD there hardly reaches 100 m, which is much less than the estimate of above 500 m, derived from climatology (cf Fig. 15 of Griffies et al. 2009).

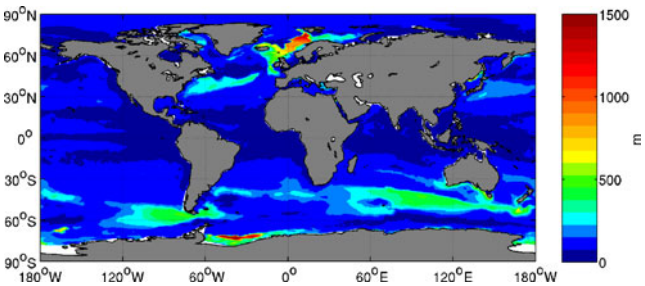

Fig. 9 Maximum mixed layer depth during the last 10 years of the model simulation computed as a maximum of monthly averaged values

The MLD of about 300 m is found in the Gulf Stream and in some places over the ACC. This qualitatively agrees with the other models and observations. A thick mixed layer is also found at the southern edge of the basin in the Weddell Sea. This artifact is not present in observations but is shared by most CORE I models (except for NCAR-POP and KNMI-MICOM).

4 Conclusions

Given the new design technology of FESOM, its ability to simulate the global ocean circulation with the skill of other models of similar resolution is far from being evident. The main motivation for this study was thus to demonstrate that the ocean state simulated by FESOM is close to that reproduced by other coupled ocean-ice models. By following the procedure and performing diagnostics of Griffies et al. (2009) we show that this is indeed the case: the ocean state simulated with FESOM is largely within the spread reported in Griffies et al. (2009).

The setup used by us intentionally does not exploit the full unstructured mesh potential of FESOM (the ratio of the largest to the smallest mesh size is only about 10, close, for example, to that of MPI model).

In such circumstances FESOM lags behind structured-mesh models of same resolution in terms of numerical efficiency, as discussed, for example, in Danilov et al. (2008). Its strength, however, lies in the ability to provide local refinement without nesting, a task where mesh degrees of freedom can be used by FESOM very efficiently. We see the analysis reported here as a necessary step in establishing this approach. It contributes to the understanding of long-term model behavior, which is a prerequisite for interpreting model results in future applications.

The work carried in this study also provided important feedbacks to further model development. The major modification was introduced to the implementation of Redi/GM schemes (see Section 2). Although the improvement is significant, some inconsistency between the computation of isopycnal slope (on prisms) and the computation of Redi/GM fluxes (on tetrahedral elements, as implied by the model discretization) is introduced, which can have an impact on climate scale simulations (Griffies et al. 1998). More work is required to fully understand and solve this problem.

The results obtained in this study point out to the weakness of the equatorial undercurrent and the thinness of the mixed layer in the Labrador Sea. They draw our attention to other details of our numerical core and parametrizations. When judging from this perspective, we see the contribution of this work as stimulating the development of unstructured mesh ocean sea-ice models that can be used for climate studies.

Acknowledgements This work was supported by the Helmholtz Climate Initiative REKLIM (Regional Climate Change). The computational resources for this work were provided through the North-German Supercomputing Alliance (HLRN). We are indebted to Martin Losch and Ralph Timmermann for discussions and advice.

References

Cavalieri DJ, Parkinson CL, Vinnikov KY (2003) 30-Year satellite record reveals contrasting Arctic and Antarctic decadal sea ice variability. Geophys Res Lett 30(18). doi:10.1029/2003GL018031

Conkright ME, Levitus S, Antonov JI, Baranova O, Boyer TP, Garcia HE, Gelfeld R, Johnson D, Locarnini RA, O'Brien TD, Smolyar I, Stephens C (2002) World ocean database 2001 and world ocean atlas 2001. American Geophysical Union, Washington

Cunningham SA, Kanzow T, Rayner D, Baringer MO, Johns WE, Marotzke J, Longworth HR, Grant EM, Hirschi JJM, Beal LM, Meinen CS, Bryden HL (2007) Temporal variability of the Atlantic meridional overturning circulation at 26.5N. Science 317:935–938

Danilov S, Kivman G, Schröter J (2004) A finite-element ocean model: principles and evaluation. Ocean Model 6(2):125–150. doi:10.1016/S1463-5003(02)00063-X

Danilov S, Wang Q, Losch M, Sidorenko D, Schröter J (2008) Modeling ocean circulation on unstructured meshes: comparison of two horizontal discretizations. Ocean Dynamics 58:365–374. doi:10.1007/s10236-008-0138-5

Gent PR, McWilliams JC (1990) Isopycnal mixing in ocean circulation models. J Phys Oceanogr 20:150–155

Griffies SM (1998) The GentMcWilliams skew flux. J Phys Oceanogr 28:831–841

Griffies SM, Gnanadesikan A, Pacanowski RC, Larichev VD, Dukowicz JK, Smith RD (1998) Isoneutral diffusion in a z-Coordinate Ocean Model. J Phys Oceanogr 28(5):805–830. doi:10.1175/1520-0485(1998)028<0805:IDIAZC>2.0.CO;2

Griffies SM, Biastoch A, Böning C, Bryan F, Danabasoglu G, Chassignet EP, England MH, Gerdes R, Haak H, Hallberg RW, Hazeleger W, Jungclaus J, Large WG, Madec G, Pirani A, Samuels BL, Scheinert M, Gupta AS, Severijns CA, Simmons HL, Treguier AM, Winton M, Yeager S, Yin J (2009) Coordinated ocean-ice reference experiments (cores). Ocean Model 26(1–2):1–46. doi:10.1016/j.ocemod.2008.08.007

Johnson GC, Sloyan BM, Kessler WS, McTaggart KE (2002) Direct measurements of upper ocean currents and water properties across the tropical pacific during the 1990s. Prog Oceanogr 52:31–61

Large WG, Yeager SG (2004) Diurnal to decadal global forcing for ocean and sea-ice models: the data sets and flux climatologies. NCAR, technical Report TN-460+STR

Pacanowski R, Philander S (1981) Parameterization of vertical mixing in numerical models of tropical oceans. J Phys Oceanogr 11:1443–1451

Redi MH (1982) Oceanic Isopycnal Mixing by Coordinate Rotation. J Phys Oceanogr 12(10):1154–1158. doi:10.1175/1520-0485(1982)012<1154:OIMBCR>2.0.CO;2

Timmermann R, Hellmer H, Beckmann A (2002) Simulations of ice-ocean dynamics in the weddell sea 2. Interannual variability 1985–1993. J Geophys Res 107. doi:10.1029/2000JC000742

Timmermann R, Danilov S, Schröter J, Böning C, Sidorenko D, Rollenhagen K (2009) Ocean circulation and sea ice distribution in a finite element global sea ice-ocean model. Ocean Model 27(3–4):114–129. doi:10.1016/j.ocemod.2008.10.009

Trenberth KE, Caron JM (2001) Estimates of meridional atmosphere and ocean heat transports. J Climate 4(16):3433–3443. doi:10.1175/1520-0442(2001)014<3433:EOMAAO>2.0.CO;2

Wang Q, Danilov S, Schröter J (2008) Finite element ocean circulation model based on triangular prismatic elements, with application in studying the effect of topography representation. J Geophys Res 113(2):21. doi:10.1029/2007JC004482

Whitworth T (1983) Monitoring the transport of the antarctic circumpolar current at drake passage. J Phys Oceanogr 13:2045–2057

Whitworth T, Peterson R (1985) Volume transport of the antarctic circumpolar current from bottom pressure measurements. J Phys Oceanogr 15:810–816

Whitworth T, Nowlin W, Worley S (1982) The net passage of the antarctic circumpolar current through drake passage. J Phys Oceanogr 12:960–971

Willebrand J, Barnier B, Böning C, Dieterich C, Killworth PD, Provost CL, Jia Y, Molines JM, New AL (2001) Circulation characteristics in three eddy-permitting models of the north atlantic. Prog Oceanogr 48(2–3):123–161. doi:10.1016/S0079-6611(01)00003-9